Heat Transfer During Microwave Combination Heating: Computational Modeling and MRI Experiments

Vineet Rakesh
Dept. of Biological and Environmental Engineering, Cornell University, Ithaca, NY 14853

Youngseob Seo
Dept. of Biomedical Engineering, University of California, Davis, CA 95616

Ashim K. Datta.
Dept. of Biological and Environmental Engineering, Cornell University, Ithaca, NY 14853

Kathryn L. McCarthy and Michael J. McCarthy
Dept. of Food Science and Technology, University of California, Davis, CA 95616

DOI 10.1002/aic.12162
Published online January 25, 2010 in Wiley Online Library (wileyonlinelibrary.com).

Combination of heating modes such as microwaves, convection, and radiant heating can be used to realistically achieve the quality and safety needed for cooking processes and, at the same time, make the processes faster. Physics-based computational modeling used in conjunction with MRI experimentation can be used to obtain critical understanding of combination heating. The objectives were to: (1) formulate a fully coupled electromagnetics - heat transfer model, (2) use magnetic resonance imaging (MRI) experiments to determine the 3D spatial and temporal variation of temperatures and validate the numerical model, (3) use the insight gained from the model and experiments to understand the combination heating process and to optimize it. The different factors that affect heating patterns during combination heating such as the type of heating modes used, placement of sample, and microwave cycling were considered. Objective functions were defined and minimized for design and optimization. The use of such techniques can lead to greater control and automation of combination heating process benefitting the food process and product developers immensely. © 2010 American Institute of Chemical Engineers *AIChE J,* 56: 2468–2478, 2010
Keywords: combination heating, electromagnetics, magnetic resonance imaging, finite element method, heat transfer, objective functions

Introduction and Objectives

Increased speed of food preparation along with improved quality and safety of the final product is critical to food processing for both domestic and industrial processes. A number of heating techniques are currently used to prepare foods. However, each heating method produces its own characteristic heating profile leading to different speed, quality, and safety issues depending on the heating method used. Combining different heating modes on the other hand can potentially provide customized heating profile suitable for a particular process. At the same time, combination heating can help speed up the heating process. Using microwaves with convection and radiation, known as microwave

Correspondence concerning this article should be addressed to A. K. Datta. at akd1@cornell.edu.

combination heating, is one such novel combination heating technique that has been found to be effective. However, systematic development, design, and optimization of microwave combination heating requires comprehensive knowledge of the engineering fundamentals that govern the relationship between combined modes of heating and the final quality and safety of the prepared food. Physics-based computational modeling used in conjunction with novel experimentation can provide a level of understanding of the combination heating process that may be impossible to achieve either by modeling or experiments alone. A detailed study of combination heating using computations and experiments that is needed for critical understanding of the process is not present in literature.

Development of combination heating requires a detailed study of processing variables and food factors. Processing variables are the factors related to the combination oven such as types of modes combined, and the power levels and cycling of the different modes. Although researchers have studied different combinations such as microwave-convection,[1–3] microwave-jet impingement,[4,5] and microwave-infrared[6–8] using experimental and/or numerical techniques, a comprehensive work that looks into the different oven parameters mentioned earlier and does a comparative study of different combinations starting from fundamental physics is missing. Sample factors refer to the properties of the sample being heated and the transport processes occurring inside. Again, a detailed study that looks at the spatial variation of heating profiles through simulation and elaborate experiments has not been accomplished. Majority of the combination heating studies[1,2,9] have not looked at spatial heating, being concerned more with the overall drying rate as the application area.

In this study, we use physics-based computational model to investigate the different processing variables and food factors and how they affect the final quality of the prepared food. Two-way coupling of electromagnetic heating and heat transfer is needed for accurate description of the process as the properties of food (dielectric and thermal) change with temperature. Implementation of this two-way coupling in 3D presents inherent challenges and has been rarely implemented[10,11] and, moreover, these studies have not looked at microwave combination heating. Validation of the computational model is critical, more so since the combination heating technique involves volume heating due to microwaves that is spatially nonuniform. Elaborate measurement techniques such as Magnetic Resonance Imaging (MRI),[12–14] that presents a precise picture of the heating profiles in 3D, have not been used earlier for validation of computational models. We use novel experiments based on MRI to obtain 3D spatial variation of heating in the samples to validate the numerical model and complement understanding. The quality of the product obtained after a cooking process is defined by the temperature inside the sample and is a result of the processing variables and food factors. Although both heat and mass (water) transfer occur inside the food during the heating process, we have limited the analysis to heat transfer to focus more on the processing variables.

The specific objectives of the work are: (1) formulation and implementation of a fundamental physics-based fully coupled electromagnetics - heat transfer model to study microwave combination heating, (2) use of MRI experiments to determine the 3D spatial and temporal variation of temperatures obtained during combination heating, (3) quantitative comparison of the computed results with the MRI data, (4) use the insight gained from the model and experiments to understand the process of combination heating comprehensively and to thereby optimize the process.

Methods

Mathematical description of the microwave combination heating process, MRI methodology used, and experimental measurement of the input parameters are now discussed.

Mathematical description

Solution of the microwave combination heating problem involves two different physics: electromagnetics and transport. The Maxwell's equations of electromagnetics need to be solved to determine the electric field inside the oven cavity and sample. Knowing the electric field distribution inside the sample, power absorbed at any location can be determined. As discussed earlier, transport is limited to heat transfer. The heat balance equation is then solved using the source term for microwave heating to determine the temperatures inside the sample. This process is repeated, i.e., solution of Maxwell's equations followed by heat transfer, to incorporate changes in the dielectric properties as the temperatures change. Thermal properties are also functions of temperature and this is incorporated while solving the energy equation.

Electromagnetics. The Maxwell's equations of electromagnetics are given by:

$$\nabla \times \mathbf{E} = -j\omega\mu_0\mathbf{H} \tag{1}$$

$$\nabla \times \mathbf{H} = j\omega\varepsilon_0\varepsilon\mathbf{E} \tag{2}$$

$$\nabla \cdot \varepsilon\mathbf{E} = 0 \tag{3}$$

$$\nabla \cdot \mathbf{H} = 0 \tag{4}$$

where $\mathbf{E}$ is the electric field intensity and $\mathbf{H}$ is the magnetic field intensity.

The dielectric constant, ε', and the dielectric loss factor, ε'', are both functions of temperature. The complex relative permittivity, ε, is written as:

$$\varepsilon = \varepsilon'(T) + j\varepsilon''(T) \tag{5}$$

Boundary Condition. The oven walls are perfect electric conductors. Therefore,

$$E_{\text{tangential, oven wall}} = 0 \tag{6}$$

Microwave Heating Term. Heat absorbed by the sample per unit time due to the microwaves is given by:

$$Q(x, y, z, t) = \frac{1}{2}\omega\varepsilon_o\varepsilon''|\mathbf{E}|^2 \tag{7}$$

Table 1. Input Parameters for the Computations

Parameter	Value
Oven dimensions (m)	0.6096 × 0.4445 × 0.4445
Sample (cylindrical) dimensions (m)	0.038 (dia) × 0.036
Thermal conductivity, k (W/m K)	0.5313 + 0.002T
Specific heat, c_p (J/kg K)	3724.4 + 2.0839T
Density, ρ (kg/m^3)	1000
Microwave frequency (GHz)	2.45
Dielectric constant, ε'	66.987 + 0.1553T − 0.0011T^2
Dielectric loss, ε''	13.247 + 0.0693T + 0.0003T^2
Heat transfer coefficient, h (W/m^2 K)	
Top surface (Settings I and III)	22
Top surface (Settings II and IV)	35
Curved surface (Settings I, II, III, and IV)	20
Air temperatures (°C)	
Combinations I and III	80
Combinations II and IV	110

Heat Transfer. The sample inside the oven is heated volumetrically by microwaves. Heat conduction occurs inside the sample.

$$\rho c_p \frac{\partial T}{\partial t} = \nabla \cdot (k \nabla T) + Q(x, y, z, t) \tag{8}$$

Boundary Conditions. Convection and radiant heating act only on the surface and are, therefore, included as boundary conditions.

$$-k \frac{\partial T}{\partial n}\bigg|_{\text{surface}} = h(T - T_{\text{air}}) \tag{9}$$

where n is the direction normal to a particular surface of the sample, h is the transfer coefficient due to convection and radiant heating at that surface (determined through experiments), and T_{air} is the oven air temperature.

Input Parameters. Dielectric properties of the samples (ε', ε'') as functions of temperature were determined experimentally using the HP85070 open ended coaxial high temperature probe (Agilent Technologies, Palo Alto, CA). Thermal properties (k, c_p) were measured as functions of temperature using the KD2 Pro probe (KD2, Decagon Devices, Pullman, WA). Surface heat transfer coefficients for different heating combinations were obtained by measuring point temperature using thermocouples and heat flux using the heat flux sensors (HFS-3, Omega, Stamford, CT) connected to FLUKE data acquisition Bucket (Fluke Everett, WA). All input parameters are shown in Table 1.

Solution of Governing Equations. The schematic of the computational domain along with the different physics solved for in the subdomains are shown in Figure 1. The governing equations for electromagnetics and heat transfer are fully coupled. As temperatures in the sample change due to heating, the dielectric properties change as given in Table 1. This in turn changes the electric field distribution inside the oven and sample and as a result, the microwave power absorbed (source term in the heat equation) by the sample changes and electromagnetic simulations need to be performed again to determine the updated microwave source term. The governing equations for the two physics were solved using the finite element method in the commercial solver, COMSOL Multiphysics (COMSOL Burlington, MA). To incorporate the coupling during the solution process, the electromagnetics and heat transfer problems were independently set up in the solver and a code was then written in COMSOL Script to implement the feedback mechanism. The electromagnetics problem was solved using the GMRES iterative solver with the Geometric Multigrid preconditioner. The mesh for the electromagnetic problem consisted of a

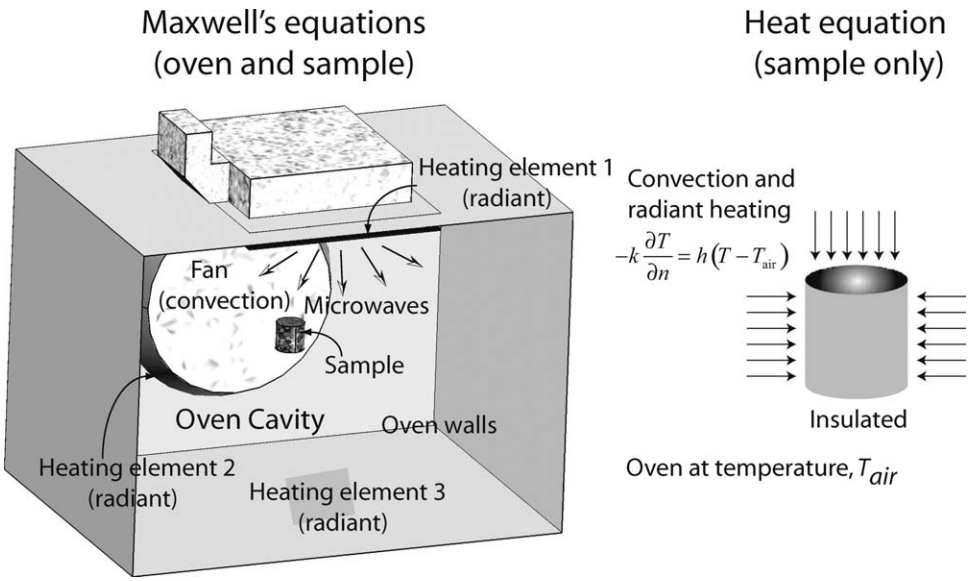

Figure 1. (a) The computational domain for the electromagnetic simulation (for microwave heating) consists of both the oven and the sample; (b) heat transfer was solved only inside the food as shown.

Also, shown are the boundary conditions used on the surface of the food sample to simulate convection and radiant heating.

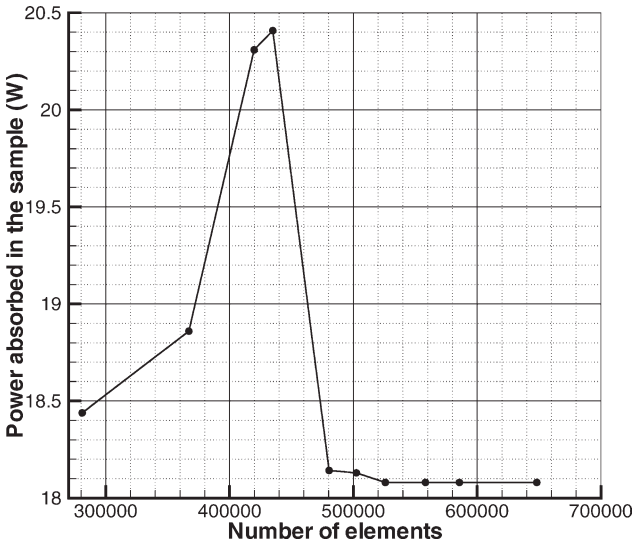

Figure 2. Mesh convergence analysis for the electromagnetic modeling.

The total number of elements chosen for the final solution was 525,873.

total of 525,873 quadratic tetrahedral elements (with 74,005 elements in the sample) based on mesh convergence study as shown in Figure 2. It was ensured that the mesh consisted of more than five elements per wavelength both in the cavity and the sample. For solving the energy equation, the UMFPACK direct solver was used with the sample discretized into 10,980 elements. The coupling parameters consisting of solver selection for the two physics, solution update interval and mapping of the electromagnetic solution to the heat transfer mesh and vice versa were programed in the code. The simulations were run on a 3 GHz Windows workstation with 16 Gb memory.

Magnetic resonance imaging

Combination Heating Modes. Convection and radiant heating modes were combined with microwaves for the study. Different combinations of these heating modes corresponding to different processing conditions were considered. The different processing conditions included combination of different oven temperatures, heat transfer rates, and microwave power cycling. These are listed in Table 2. The combinations were programed in a GE Profile Trivection oven (Model no. JT930BHBB, General Electric Company, Louisville, KY).

Sample Preparation. The food analog used for the study was prepared by mixing TX151 powder (Oil Center Research International, Lafayette, LA) with water (1:10 parts by weight). When mixed with water the polymer forms a gel that maintains its integrity during heating. The solution was poured into 50 mL beakers and heated to 70° C in a water bath for 55 min to initiate gelation. Samples were cooled to room temperature and allowed to equilibrate at least 24 h before heating.

MRI Methodology. The magnetic resonance imaging experiments were performed using a ~7T super-conducting magnet and Biospec console (Bruker Biospin MRI Billerica, MA) with 300 MHz for ^{1}H-resonance frequency. Gradient echo sequence (Fast Low Angle Shot, FLASH) magnetic resonance imaging protocol was used to generate the temperature maps. The detailed MRI parameters are given in Table 3. MRI data was acquired for each sample at room temperature and then after heat treatment. The samples were positioned identically in the magnet for the imaging procedure before and after heat treatment. The MRI data acquisition time was 9 s. Temperature maps for different durations of heating using different combinations were obtained using MRI. The temperature maps represented 10 horizontal slices from the bottom to top of the cylindrical sample. Temperatures at the different locations are calculated using the following expression:

$$\Delta T = \frac{\phi - \phi_{\text{ref}}}{\alpha\gamma(\text{TE})B_{\text{o}}} \tag{10}$$

where ϕ is the phase shift, B_{o} is the magnetic field strength, α is the proportionality constant, TE is the echo time, and γ is the magnetogyric ratio of hydrogen nucleus.

MRI measurements were done for four different combinations of heating modes. The different heating modes along with the times at which the MRI measurements were performed are shown in Table 2. The heating times were chosen so that there was negligible moisture transport for the heating duration as discussed in next section. As shown in Table 2, heating times for heating combinations I and III were up to 12 min. For heating combinations II and IV, heating times were restricted to 2 min as these combination provided higher heating rates and there was rapid temperature rise in the samples.

Moisture Loss Measurement. Moisture loss due to the heating process was determined using gravimetric measurement. Each sample was weighed before heating at room

Table 2. The Different Combinations of Heating Modes and MRI Measurements Times

Heating Combination	Heating Modes Used	Convection Temperature (°C)	MRI Measurement Times (min)
I	Convection, Radiant	80	2, 4, 6, 8, 10, 12
II	Convection, Radiant	110	0.5, 1, 1.5, 2
III	Convection, Radiant, Microwave (Cycling: 10 s on, 40 s off)	80	2, 4, 6, 8, 10, 12
IV	Convection, Radiant, Microwave (Cycling: 20 s on, 10 s off)	110	0.5, 1, 1.5, 2

Table 3. MRI Parameters for the Experiments

Parameter	Value
Echo time (TE)	3.264 ms
Repetition time (TR)	89.6 ms
Flip angle	20°
Matrix size	128 × 128
Field of view (FoV)	55 × 55 mm^2
Number of slices	10 (Coronal slice)
Slice thickness	3 mm

temperature and immediately following the combination heating process. It was confirmed that moisture transport was negligible.

Results and Discussions

The mathematical model is validated using experimental data and the results are discussed. Different oven parameters are considered and techniques to optimize and design different food processes using combination heating are discussed.

Validation of mathematical model using MRI results

The temperatures predicted from the mathematical model were compared with those measured using MRI for experimental validation. To provide a comprehensive and quantitative validation, average temperatures and spatial temperature distributions were compared. Comparison of average temperatures, although a good method for quantitative validation of the computational model, does not provide insight into the spatial temperature distribution. For heating combinations involving microwaves that heat the sample non-uniformly, comparison of spatial temperature distribution is critical for accurate validation of the numerical model.

Comparison of Average Temperature Rise. Comparison of average temperatures in the sample obtained from computations and MRI for the different heating combinations are shown in Figure 3. A good match between computed and experimental temperature histories can be seen for all heating combinations. As expected, for combinations involving additional modes of heating (Combinations III and IV as compared to Combinations I and II, respectively), average temperature rise is greater.

Comparison of Spatial Temperature Distribution. Spatial temperature maps obtained from the model were compared to those measured by MRI at different times for various heating combinations as shown in Figure 4. The temperatures were compared at six horizontal slices (perpendicular to axis) across the cylindrical sample. As mentioned earlier, 10 slices were obtained from MRI. The six comparison slices were chosen from the center of the gel sample. Slices at the top and bottom of the sample were not used for comparison since these have partial volume effects and slightly non-ideal surfaces. Any changes in sample geometry related to heating will also primarily impact these areas and, hence, they have been omitted from the detailed spatial comparison.

Figures 4–7 demonstrate a good match between the simulated and experimental spatial temperature profiles obtained by heating the samples using Combinations I–IV, respectively. Samples were manually positioned inside the oven and into a specially constructed sample shuttle for the MRI spectrometer. Sample positioning inside the over is accurate to less than 1×10^{-4} m in the vertical direction and less than 5×10^{-3} m in the horizontal directions. Sample positioning in the MRI spectrometer is accurate to within 1×10^{-4} m in all directions. Positional differences in the oven lead directly to differences in heating related to the spatial variation of the electromagnetic radiation. Positional differences in the MRI spectrometer would result in minor impacts on the temperature calculations. Hence, dissimilarities in the computed and experimental profiles are primarily related to variations in sample placement combined with variations in sample physical properties. Variations in sample physical properties would result from the inclusion of air bubbles and non-uniform solid distributions. The effect of changes in sample position inside the oven cavity on heating is presented in detail in a later section.

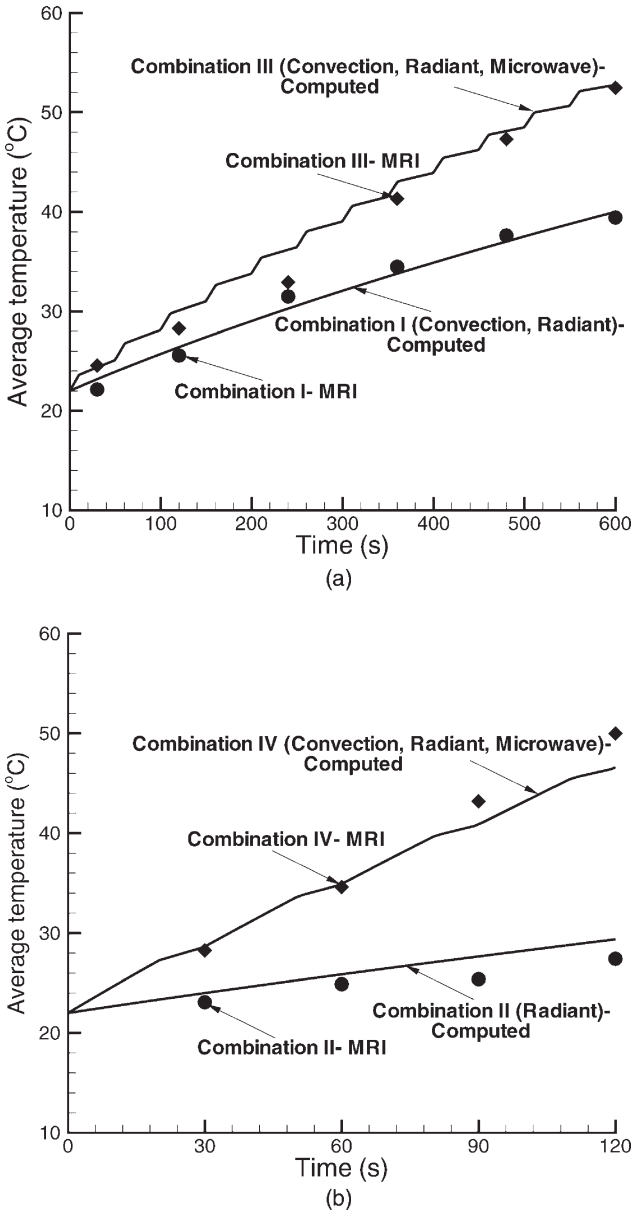

Figure 3. Comparison of average temperatures in the sample obtained from computations and MRI for the various heating combinations shown in Table 2 after different time intervals.

(a) With oven temperature at 80°C and (b) with oven temperature at 110°C. The computations were done at Cornell University and MRI measurements at UC, Davis.

Two distinct features of heating are observed: surface heating due to convection and radiation as can be seen in Figures 4 and 5 (which do not involve microwave heating) and heating at the interior locations in addition to surface heating as seen in Figures 6 and 7. These two features of

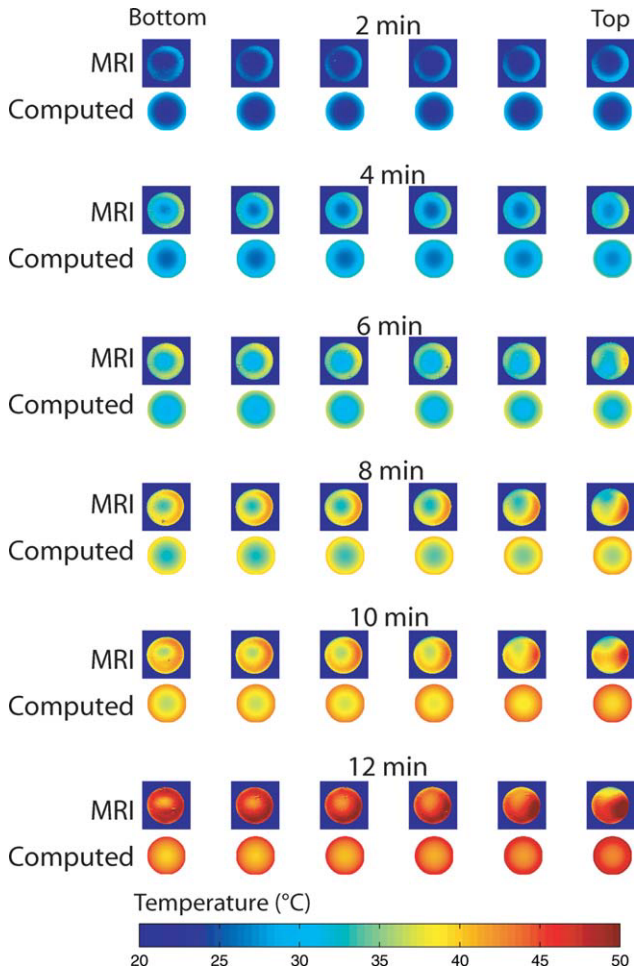

Figure 4. Spatial temperature maps obtained from the mathematical model compared to those measured by MRI at six different times for the sample heated by Combination I.

The temperatures are compared at six different slices across the cylindrical sample starting from the bottom slice on the left to the top slice on the right. The initial temperature of the samples was 22°C. [Color figure can be viewed in the online issue, which is available at wileyonlinelibrary.com.]

heating nicely complement each other so that for heating combinations that include all the different modes of heating (Combinations II and IV), the entire sample heats more uniformly (Figures 6 and 7).

The similarities of the heating patterns between measured and computed are striking for all combinations. Combination I in Figure 4 demonstrates symmetric heating with only slightly non-symmetric heating in the gel sample. For Combination II heating in Figure 5, the MRI and computed spatial temperature maps are nearly identical, detailing the power of the computational model. In Combinations III and IV (Figures 6 and 7), the comparison is best at shorter times and the non-uniform heating induced by the electromagnetic radiation is evident in both the model and experimental data. At the longer heating times (12 min and 120 s) for both Combination III and IV, respectively, preferential heating on one side of the sample is observed in the computation and seen in the experimental measurements. The experimental measurements also demonstrate some spatial differences from the computational model at longer times, however, these are primarily related to the difficultly in matching identically the computation to the actual sample placement in the oven. Most importantly, the model correctly predicts a number of features of the 3D heating profiles seen in the experimental data as a result of non-uniform microwave fields.

Convection and radiant heating and combination with electromagnetic heating

As discussed in the previous section, different heating combinations result in different heating patterns inside the sample. By combining volumetric and surface heating appropriately, one can obtain desired temperature profiles inside the sample and at the same time speed up the heating process. Convection and radiation heating modes heat mostly near surface as shown in Figure 8. Change in the oven temperature and movement of the fan (velocity, direction of rotation) changes the heating profiles due to these two modes of heating. Figure 8 (top figures) shows the temperature profile along the horizontal centerline of the sample for convective and radiant heating at two different oven temperatures (80°C and 110°C). For an oven temperature of 110°C, the heating is faster as expected. The temperature profiles are symmetric about the center and maximum heating is near the surface. On addition of microwaves (bottom figures), heating in the corresponding combinations are faster and the temperature profiles are no longer symmetric with the right side of the sample heating faster demonstrating the

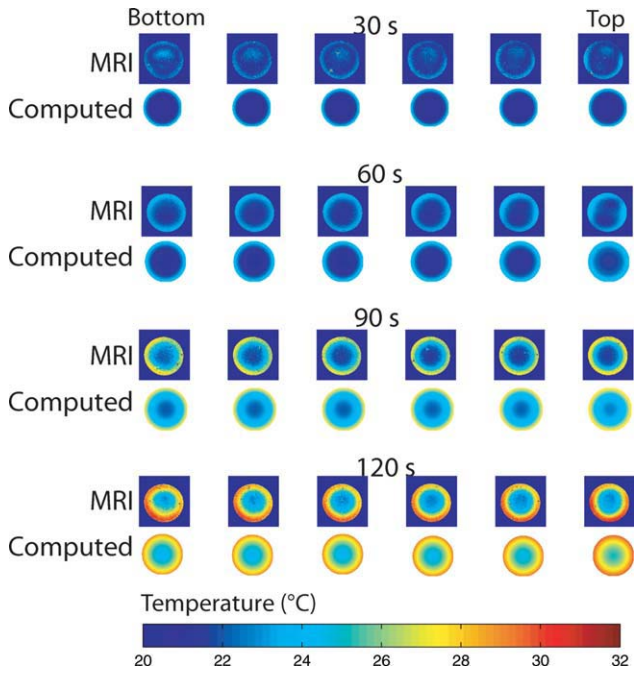

Figure 5. Spatial temperature maps obtained from the mathematical model compared to those measured by MRI at four different times for the sample heated by Combination II.

[Color figure can be viewed in the online issue, which is available at wileyonlinelibrary.com.]

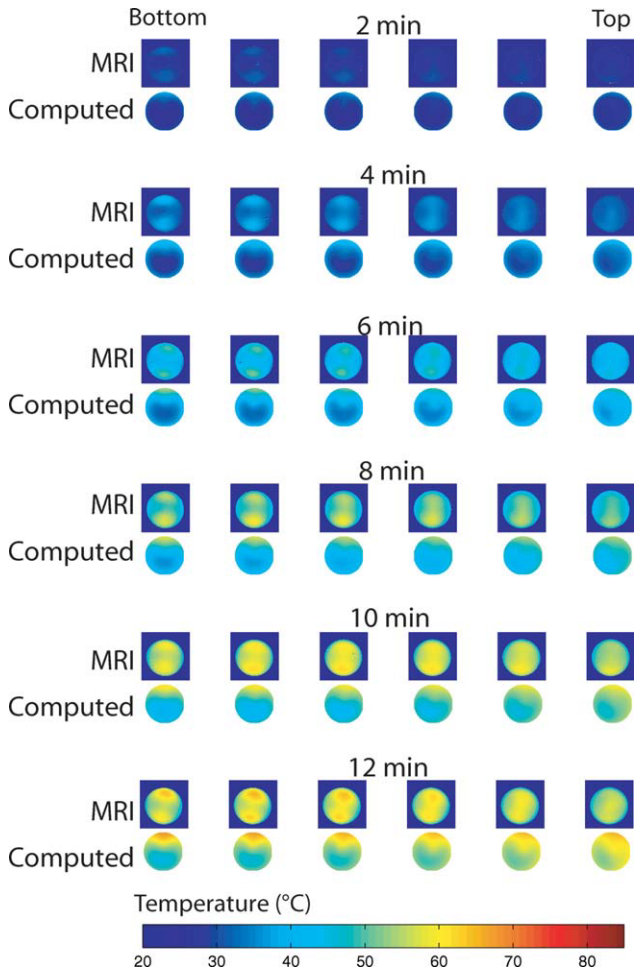

Figure 6. Spatial temperature maps obtained from the mathematical model compared to those measured by MRI at six different times for the sample heated by Combination III.

[Color figure can be viewed in the online issue, which is available at wileyonlinelibrary.com.]

volumetric electromagnetic heating, also seen in Figures 6 and 7. By estimating the relative temperature rise due to each heating mode, guidelines for combining different modes of heating can be formulated based on the processing needs. Such combinations can be particularly important in speeding up cooking processes where high temperatures are desired at the surfaces of the food so that browning and crust formation occurs and at the same time the interior needs to be heated adequately.

Electromagnetic heating patterns: Effect of positioning of sample inside the oven cavity

The heating profiles due to combination heating are the consequences of volumetric electromagnetic heating and surface heating due to convection and radiation. The electromagnetic heating patterns inside an oven cavity is a function of the electric field, given by Eq. 7. Figure 9a presents the electric field distribution in the oven cavity with the sample placed at the center. It can be observed that regions of high and low electric fields are obtained inside the oven alternately. This type of electric field patterns in turn leads to hot and cold spots in the sample, also shown in Figure 9a. Change in location of the sample changes the pattern of the electric field distribution inside the oven cavity significantly due to change in resonance pattern of the electromagnetic waves. To demonstrate this effect of change in location of the sample on the electric field patterns inside the cavity and the sample, the sample was displaced horizontally inside the oven by 10 cm toward the front of the center and the electric field patterns were calculated using the model by solving the Maxwell's equations. Figure 9b shows that there is considerable change in electric field patterns both inside the oven and sample. Especially in the sample, it can be observed that the region of high electric filed shifts from the top of the sample to the bottom, as the sample is displaced. Going back to Figures 6 and 7 it can be seen that these variations may change the nature of heating and it becomes almost impossible to predict these features more accurately using the computational model owing to the uncertainty of placement.

To quantify this effect of change in position, power absorbed by the sample placed at seven different locations inside the oven due to microwave heating are plotted in Figure 10. It can be observed that there is significant variation in the power levels for different positioning of the sample inside the oven. It should be noted here that there can be numerous such locations inside the oven cavity and the ideal way to analyze the effect of positioning of the sample in the oven is to perform Monte Carlo simulations, choosing the

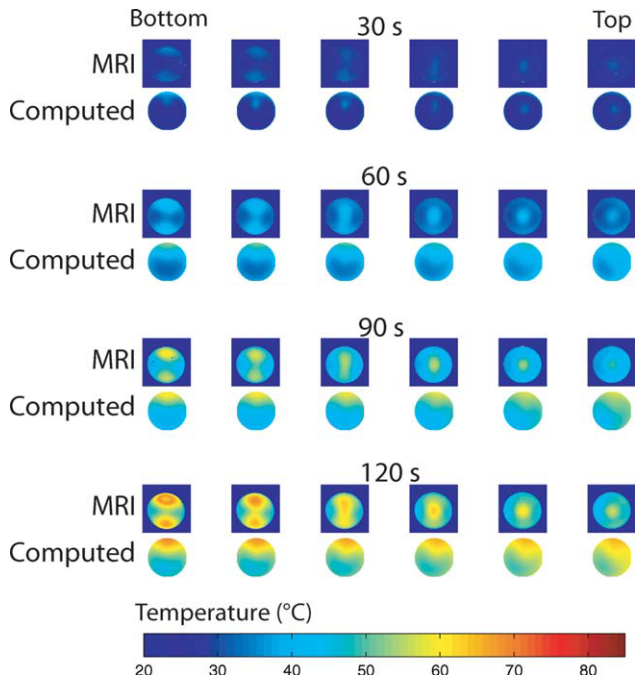

Figure 7. Spatial temperature maps obtained from the mathematical model compared to those measured by MRI at four different times for the sample heated by Combination IV.

[Color figure can be viewed in the online issue, which is available at wileyonlinelibrary.com.]

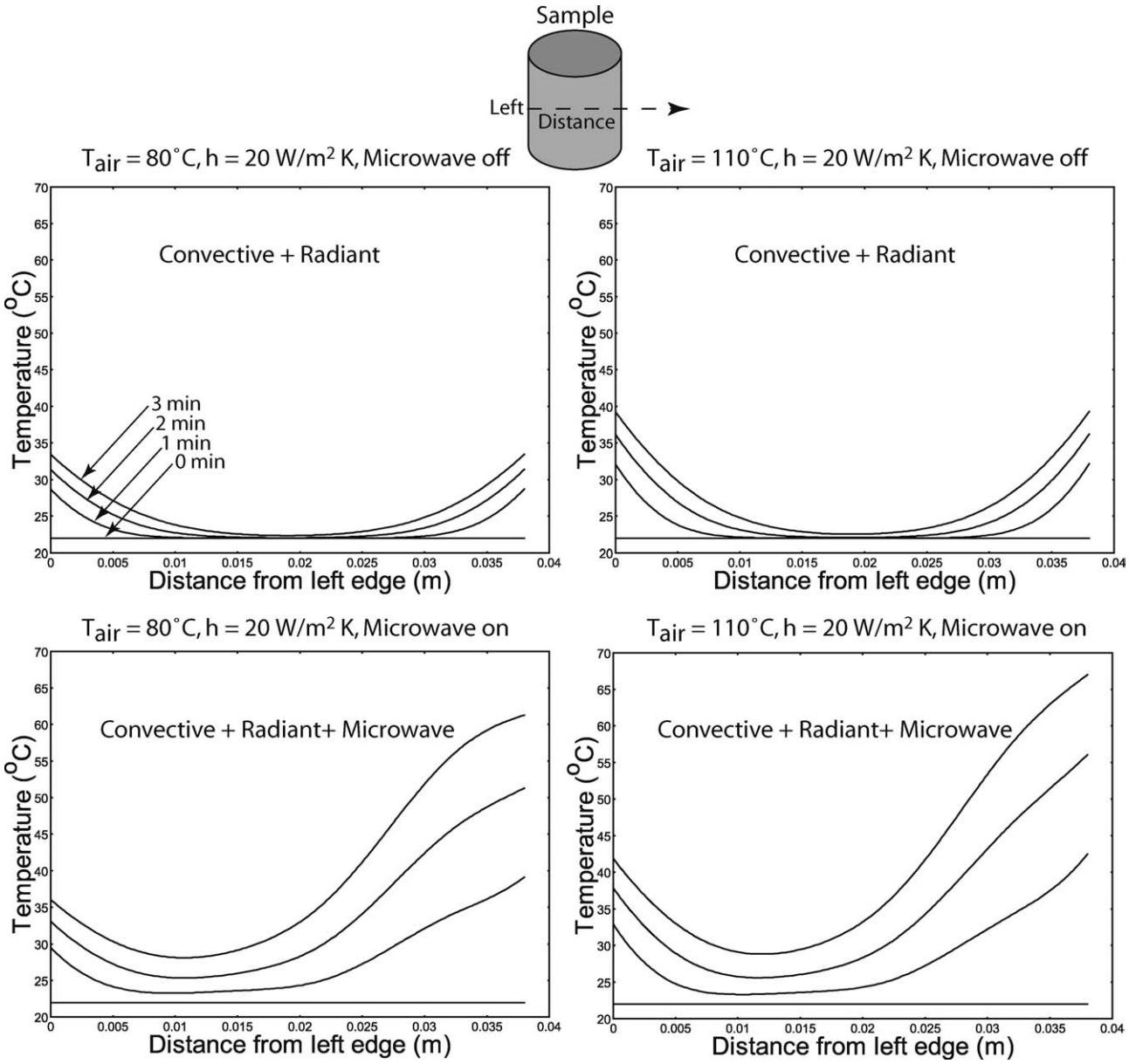

Figure 8. Heating profiles along a horizontal line at the center of the sample (as shown in the figure) for different combinations.

For each combination, curves are shown for times of 0, 1, 2, and 3 min.

sample location randomly, and analyzing the change in power absorbed by the sample (using a measure such as coefficient of variation as done in[15] for an unrelated application). However, in case of microwave heating, performing Monte Carlo simulations is not feasible since each electromagnetic simulation takes about 3 h to complete and, therefore, the full Monte Carlo analysis would require simulation times that are unrealistic. Analysis shown here with predetermined locations is a feasible approach that provides a reasonable overview of the relative change in power absorbed for the different locations of the sample inside the oven cavity.

Effect of microwave cycling

As discussed earlier, heating patterns in a sample due to electromagnetic heating are fixed for a particular location of the sample inside the oven. Heating rates inside the sample can, however, be controlled by allowing the microwave excitation to cycle. The microwaves can be made to turn off for specific intervals to allow for conductive equilibration of heat to regions that are not heated by electromagnetic heating, thereby leading to a more uniform heating of the sample. However, if a particular temperature rise and uniform heating are desired in the sample, the required cycling is not known a priori. Here, the computational model can be set as

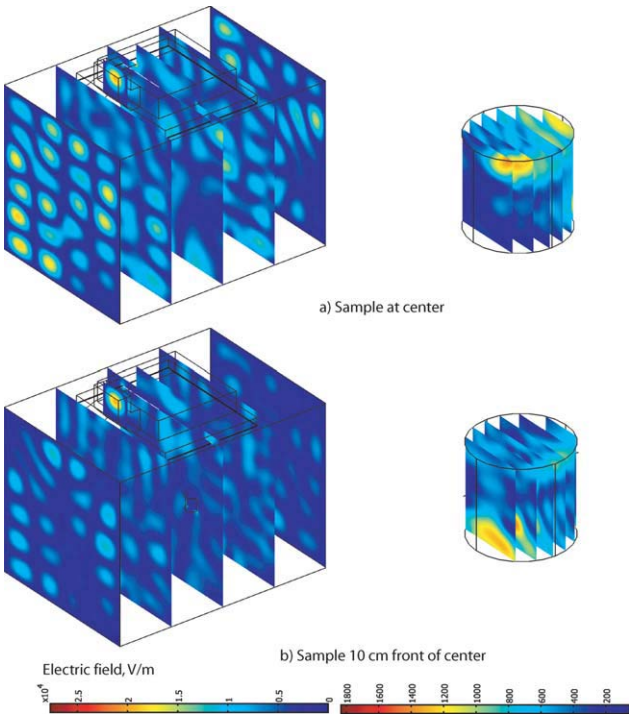

Figure 9. Electric field distribution in the oven cavity and sample for different positions of the sample inside the cavity.

(a) Sample placed at the center and (b) sample displaced 10 cm horizontally from the center toward the front of the oven. Contour colors from red to blue correspond to regions of high to low electric fields, respectively. [Color figure can be viewed in the online issue, which is available at wileyonlinelibrary.com.]

an optimization problem with an objective function to be minimized and be used to test a number of scenarios that include different periods of cycling. We choose this objective function as follows: For a particular temperature, T_p, desired for a particular process, the objective function, J, is:

$$J = \int_V F(T)dv$$

$$F(T) = \begin{cases} T - T_p & T > T_p \\ 0 & T = T_p \\ T_p - T & T < T_p \end{cases} \quad (11)$$

By definition, the value of objective function increases as the temperatures are either lower or higher than the

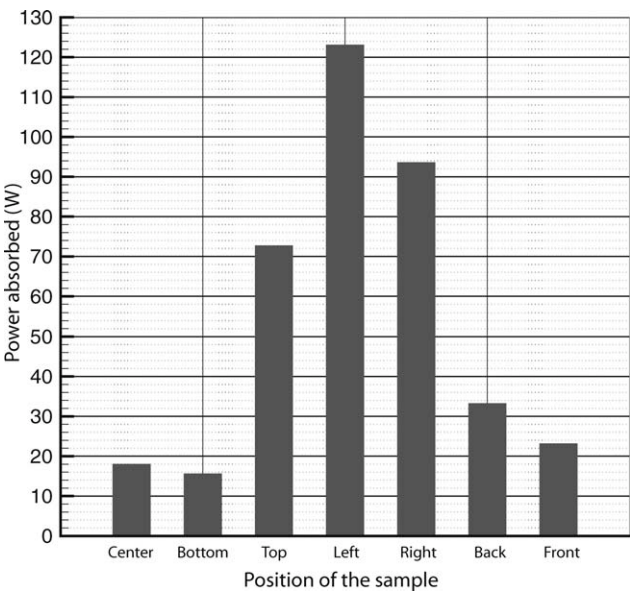

Figure 10. Total power absorbed in the food sample as a function of location inside the oven.

The sample was placed at the center and displaced by 10 cm in the three different directions as shown.

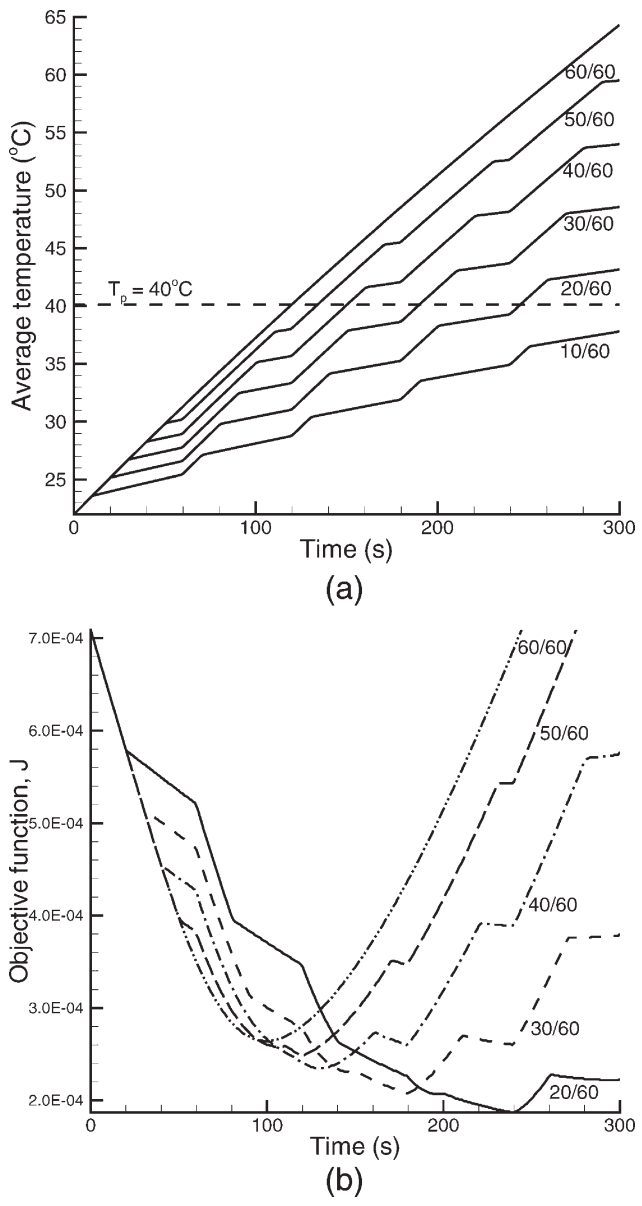

Figure 11. Average temperature rise in the sample heated using different cycles of microwave.

Also, plotted is the objective function (defined in Eq. 11) as a function of time for the cycles that reach the processing temperature of 40°C. The notation 10/60 denotes that the microwaves were on for 10 s out of a 60 s cycle.

processing temperature, T_p. Therefore, by minimizing this objective function, the best method of microwave cycling can be obtained.

A number of microwave cycling cases were considered with the same setting of convection and radiant heating and the average temperature rise in the sample and objective function were calculated and plotted as a function of time for 5 min of heating (Figure 11). The processing temperature of 40°C is reached for the five cycles with microwaves on for 20, 30, 40, 50, and 60 s out of a total cycle time of 60 s (Figure 11a). Although the average temperature rise provides an estimate of the microwave cycles that can be used, it does not provide any insight if the sample is heated uniformly to the processing temperature, T_p. Figure 11b shows that for all cycles, the objective function decreases with time as the sample starts to heat from the initial room temperature (22°C), reaches a minimum or optimum value and then starts increasing as difference in temperatures between the hot and cold locations increases. For the cycle with microwaves on for the entire duration (represented as 60/60), although the average temperature rise to 40°C is faster, the minima in the objective function curve is much higher than the cycle with microwaves on for 20 s out of a 60 s cycle. It can, therefore, be concluded that the cycle represented as 20/60 is most effective for this process as it not only leads to the final processing temperature but also provides more uniform heating. Similarly, other microwave cycles can be evaluated for different process using such an optimization technique.

In general, it is not intuitive which combination of heating modes is most efficient considering the time and quality of the final product. The microwave and surface heating patterns change with the different parameters (cycling, location, heat transfer coefficient, etc.). Use of physics-based modeling along with optimization techniques is, therefore, very important. This type of analysis can be used to design and optimize combination heating processes and can help reduce the amount of experimentation needed for product or process development.

Conclusions

A fully coupled electromagnetics heat transfer model was used in close synergy with novel MRI experimentation for comprehensive validation of the model in space and time and in turn to study the process of combination heating accurately and comprehensively. Coupling of the different physics (electromagnetics, heat transfer) presented inherent computational challenges and was accomplished by manual scripting in the computational software. Some of these difficulties include the use of different finite element meshes for the electromagnetics and heat transfer problems that required mapping of solution back and forth between the different meshes, use of different solvers for the two physics, update of material properties, and specification of coupling parameters. 3D validation of the model provided by MRI experiments with proper resolution was critical since the heating modes included volumetric electromagnetic heating.

The different factors that contribute to the heating patterns during combination heating such as heating modes used, placement of sample inside the oven, and microwave cycling were considered. The use of objective functions to design and optimize combination heating processes as described in this work can lead to greater control and automation of combination heating process benefitting the food processors and product developers immensely. Specific guidelines for processing conditions can be developed using the tools discussed in this article not only for cooking processes but also biomedical applications, wood drying, and processing of ceramics that can be optimized using microwave combination heating. As the framework consisting of the model and experimental measurement has been developed, possibilities for working with it are broad and exciting, and it can be used to provide insights into many aspects of combination heating that would not be possible otherwise.

Acknowledgments

This research was supported by grant number 2003-35503-13737 from the United States Department of Agriculture under the National Research Initiative Grant Program.

Notation

B_o = magnetic field strength, T
c_p = specific heat capacity, J/kg K
$\mathbf{E}$ = electric field intensity, V/m
h = surface heat transfer coefficient, W/m^2 K
$\mathbf{H}$ = magnetic field intensity, A/m
j = imaginary unit, $\sqrt{-1}$
J = objective function, m^{3}K
k = thermal conductivity, W/m K
n = normal direction
Q = power absorbed, W/m^3
t = time, s
T = temperature, °C
T_{air} = oven temperature, °C
T_p = processing temperature, °C
TE = echo time, s
x, y, z = directions, m
α = proportionality constant, ppm/°C
γ = magnetogyric ratio of hydrogen nucleus, rad/s T
ε = complex relative permittivity, dimensionless
ε' = dielectric constant, dimensionless
ε'' = dielectric loss, dimensionless
ε_0 = permittivity of free space, 8.854×10^{-12} F/m
μ_0 = permeability of free space, $4\pi \times 10^{-7}$ H/m
ρ = density, kg/m^3
ϕ = phase shift, rad
ω = angular frequency, rad/s

Literature Cited

1. Jumah RY, Raghavan GSV. Analysis of heat and mass transfer during combined microwave-convective spouted-bed drying. *Dry Technol*. 2001;19:485–506.
2. McMinn WAM, McLoughlin CM, Magee TRA. Microwave-convective drying characteristics of phannaceutical powders. *Powder Technol*. 2005;153:23–33.
3. Wappling-Raaholt B, Scheerlinck N, Galt S, Banga JR, Alonso A, Balsa-Canto E, Van Impe J, Ohlsson T, Nicolai BM. A combined electromagnetic and heat transfer model for heating of foods in microwave combination ovens. *J Microw Power Electromagn Energy*. 2002;37:97–111.
4. Ovadia DZ, Walker CE. Impingement in food processing. *Food Technol*. 1998;52:46–50.
5. Geedipalli S, Datta AK, Rakesh V. Heat transfer in a combination microwave-jet impingement oven. *Food Bioprod Process*. 2008;86:53–63.

6. Datta AK, Ni H. Infrared and hot-air-assisted microwave heating of foods for control of surface moisture. *J Food Eng*. 2002;51:355–364.
7. Haala J, Wiesbeck W. Modeling microwave and hybrid heating processes including heat radiation effects. *IEEE Trans Microw Theory Tech*. 2002;50:1346–1354.
8. Almeida MF. Modeling infrared and combination infrared-microwave heating of foods in an oven, PhD Dissertation, Cornell University. 2005.
9. Ren G, Chen F. Drying of steamed Asian ginseng (Panax ginseng) roots by microwave-hot air combination. *Pharmazie*. 2000;55:124–128.
10. Ma LH, Paul DL, Pothecary N, Railton C, Bows J, Barratt L, Mullin J, Simons D. Experimental validation of a combined electromagnetic and thermal Fdtd model of a microwave-heating process. *IEEE Trans Microw Theory Tech*. 1995;43:2565–2572.
11. Zhang H, Datta AK. Coupled electromagnetic and termal modeling of microwave oven heating of foods. *J Microw Power Electromagn Energy*. 2000;35:71–85.
12. McCarthy MJ. *Magnetic Resonance Imaging in Foods*, New York, NY: Chapman and Hall, Inc., 1994.
13. Bows JR, Patrick ML, Nott KP, Hall LD. Three-dimensional MRI mapping of minimum temperatures achieved in microwave and conventional food processing. *Int J Food Sci Technol*. 2001;36:243–252.
14. Nott KP, Hall LD. Validation and cross-comparison of MRI temperature mapping against fibre optic thermometry for microwave heating of foods. *Int J Food Sci Technol*. 2005;40:723–730.
15. Halder A, Datta AK, Geedipalli SSR. Uncertainty in thermal process calculations due to variability in first-order and weibull kinetic parameters. *J Food Sci*. 2007;72:E155–E167.

Manuscript received Apr. 1, 2009, and revision received Dec. 1, 2009.